

pubs.acs.org/JACS Article

Thermodynamics of Proton-Coupled Electron Transfer at Tricopper μ -Oxo/Hydroxo/Aqua Complexes

Saikat Mondal, Weiyao Zhang, and Shiyu Zhang*



Cite This: J. Am. Chem. Soc. 2024, 146, 15036-15044



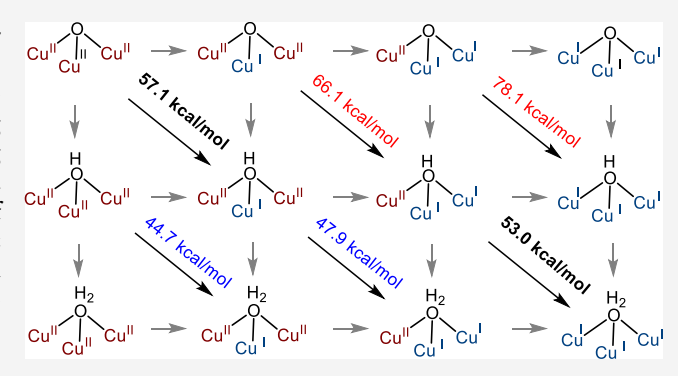
ACCESS I

Metrics & More

Article Recommendations

Supporting Information

ABSTRACT: Multicopper oxidases (MCOs) utilize a tricopper active site to reduce dioxygen to water through $4H^+$ $4e^-$ proton-coupled electron transfer (PCET). Understanding the thermodynamics of PCET at a tricopper cluster is essential for elucidating how MCOs harness the oxidative power of O_2 while mitigating oxidative damage. In this study, we determined the O–H bond dissociation free energies (BDFEs) and p K_a values of a series of tricopper hydroxo and tricopper aqua complexes as synthetic models of the tricopper site in MCOs. Tricopper intermediates on the path of alternating electron and proton transfer (ET-PT-ET-PT-ET) have modest BDFE(O–H) values in the range of 53.0–57.1 kcal/mol. In contrast, those not on the path of ET-PT-ET-PT-ET display much higher (78.1 kcal/mol) or lower (44.7 kcal/mol)



BDFE(O–H) values. Additionally, the pK_a of bridging OH and OH₂ motifs increase by 8–16 pK_a units per oxidation state. The same oxidation state changes have a lesser impact on the pK_a of N–H motif in the secondary coordination sphere, with an increase of ca. 5 pK_a units per oxidation state. The steeper pK_a increase of the tricopper center promotes proton transfer from the secondary coordination sphere. Overall, our study shed light on the PCET pathway least prone to decomposition, elucidating why tricopper centers are an optimal choice for promoting efficient oxygen reduction reaction.

■ INTRODUCTION

Multicopper oxidases (MCOs) are an important class of enzymes found in various organisms, playing crucial roles in diverse biological processes, such as copper homeostasis, electron transfer, and lignin degradation. MCOs couple the oxidation of metal or organic substrates with the four-electron reduction of O₂ to H₂O. This process is carried out with high efficiency without producing reactive oxygen species (ROS) or causing oxidative damage to the protein structure. Understanding the intricate dioxygen reduction at MCOs is of great significance in unveiling how nature harnesses the oxidative power of O₂. Heads of the protein structure oxidative power of O₂.

MCOs contain at least four copper ions: one type 1 (T1) electron-transfer site and a trinuclear copper active site (TNC) with secondary carboxylate motifs (Figure 1A). 9,10 Dioxygen reduction at MCOs involves the activation of $\rm O_2$ at fully reduced TNC, followed by 4H $^+$ 4e $^-$ proton-coupled electron transfer (PCET) to regenerate the Cu(I,I,I) state (Figure 1B). The T1 site and secondary carboxylate groups enable well-coordinated PCET during the oxygen reduction reaction (ORR). $^{10-15}$

A crucial aspect of the MCOs yet to be fully elucidated is the 4H⁺ 4e⁻ PCET (Figure 1B). Out of the 25 possible tricopper species (five oxidation states and five protonation states), only five have been characterized through spectroscopy: fully reduced (FR), resting oxidized (RO), native intermediate (NI), 6,16 peroxy intermediate (PI), 12 and alternative resting (AR). 13

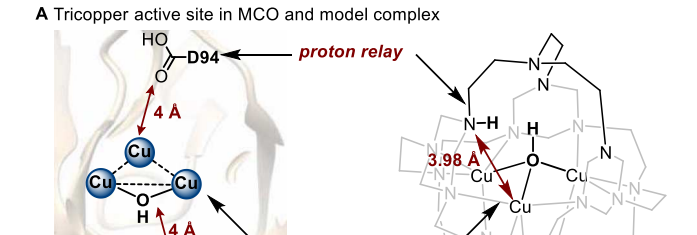
Furthermore, the thermodynamics of PCET, such as pK_a , redox potentials, and O–H bond dissociation free energies (BDFEs), remain elusive. The difficulty in measuring these values within the protein systems motivates us to study these fundamental properties using synthetic tricopper model complexes.

Recently, we reported a tricopper complex that can access all four oxidation states from $Cu^{II}Cu^{II}Cu^{II}$ to $Cu^{I}Cu^{I}Cu^{I}$. In contrast to previous synthetic models of MCOs, ^{15,18–23} this tricopper cluster is embedded in a macrocyclic TREN₄ [TREN = tris(2-aminoethyl)amine] ligand that provides a rigid coordination environment, reducing the reorganization energy of electron transfer (Figure 1C). Furthermore, we demonstrated a $2H^+$ $3e^-$ PCET from [LCu₃(I,I,I)(OH₂)]³⁺ to [LHCu₃(II,II,II)(O)]⁵⁺, where L represents the TREN₄ ligand and LH represents the protonated TREN₄ ligand. Seven intermediates were characterized to mimic the reductive regeneration of the fully reduced trinuclear copper cluster (FR) from the resting oxidized state (RO) in MCOs.²⁴

Received: December 19, 2023 Revised: May 6, 2024 Accepted: May 10, 2024 Published: May 21, 2024







edox active

Cu₃ cluster

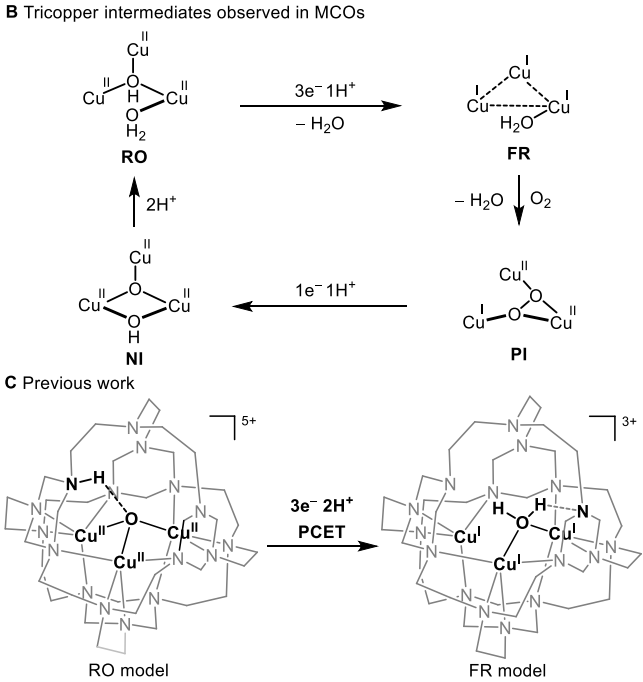


Figure 1. (A) Tricopper active site and (B) observed tricopper intermediates in MCOs. (C) Previous work on modeling the PCET at MCOs with the full encapsulated tricopper complex.^{8,2}

Importantly, a proton can transfer between the top TREN motif at the secondary coordination sphere and the tricopper center (Figure 1C). This intramolecular proton transfer is driven

	3 e⁻ holes Cu ^{II} Cu ^{II} Cu ^{II}	2 e⁻ holes Cu ^{II} Cu ^{II} Cu ^I	1 e⁻ hole Cu ^{II} Cu ^I Cu ^I	0 e⁻ hole Cu ^l Cu ^l Cu ^l
0 H ⁺	Cu Cu	Cu ^{II} Cu ^I	cul Cu cul	cu Cu Cu
1 H⁺ hydroxo	Cu Cu Cu	Cu ^{II} Cu ^I	Cu ^{II} Cu ^I	Cu Cu Cu
2 H ⁺ aqua	Cu ^{II} Cu ^{II}	Cu ^{II} Cu ^I	Cul Cul	Cu Cu Cu

Figure 2. Twelve possible tricopper intermediates for the threeelectron two-proton PCET from Cu₃(II,II,II) oxo to Cu₃(I,I,I) aqua species. The gray boxes highlight the ideal path of alternating electron and proton transfer ET-PT-ET-PT-ET.

by the basicity of the tricopper hydroxo/oxo center vs tertiary nitrogen motifs in the secondary coordination sphere, playing an important role in leveling the redox potentials from tricopper-(II,II,II) to tricopper(I,I,I).8,17

The BDFE(O-H) and pK_a of the copper oxo/hydroxo/aqua complexes can reveal the reaction landscapes of copper oxygen chemistry. Despite their significance, the BDFE(O-H) values of synthetic models of copper active sites have only been sparsely reported (Figure 3), 25-29 and no BDFE(O-H) of a tricopper complex has been measured.

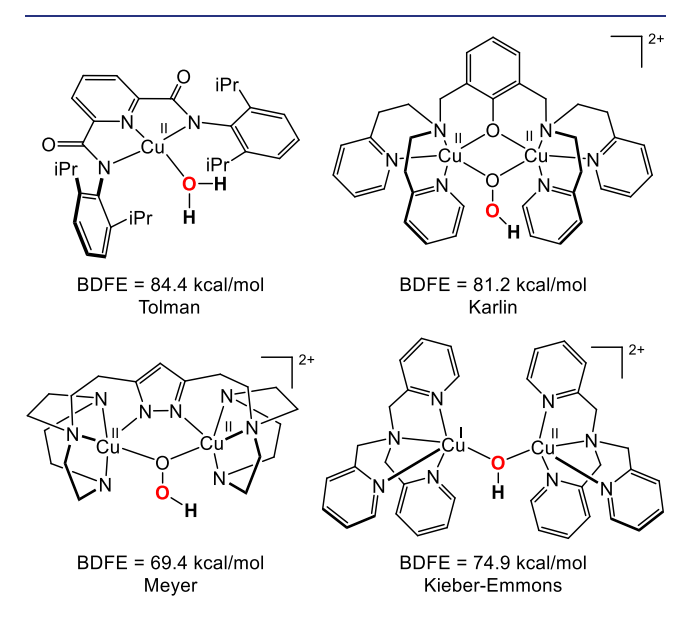


Figure 3. Previous examples of O-H BDFE measurements for monoand dicopper model complexes.

Determining the BDFE and pK_a of the O-H motifs in a TREN₄ tricopper complex presented a challenge, since the O-H protons are nested in a cage-like structure of the TREN₄ ligand. The N-H/N groups in the secondary coordination sphere complicate the p K_3 titration of OH $_2$ /OH/O groups. Due to the relatively lower steric hindrance of the N-H groups, treatment of the tricopper cluster with an acid/base often results in the protonation/deprotonation of the N/N-H group first.

Herein, we report a comprehensive analysis of BDFE and pK_a values of these tricopper hydroxo/aqua model complexes using Mayer's open-circuit potential (OCP) method. We found that the tricopper complexes on the ideal path of alternating electron and proton transfer (ET-PT-ET-PT-ET) have modest BDFE values around 53.0-57.1 kcal/mol (Figure 2, highlighted in gray). In contrast, those tricopper complexes off this ideal path have either high (78.1 kcal/mol) or lower (44.7 kcal/mol) BDFE(O-H) values. The $pK_a(O-H)$ and $pK_a(N-H)$ at different tricopper oxidation states suggest increasing driving forces of proton transfer from the secondary coordination sphere as the tricopper center is reduced from Cu₃(II,II,II) to $Cu_3(I_1I_2I)$. We discuss the implications of these BDFE and p K_a values in the context of four-electron oxygen reduction at biological tricopper centers.

RESULTS AND DISCUSSION

BDFE(O-H) of Tricopper μ -OH₂ Complexes. In our previous study, we reported the synthesis and characterization of a series of tricopper model complexes at different oxidation and protonation states.^{8,24} Building on this work, we attempt to

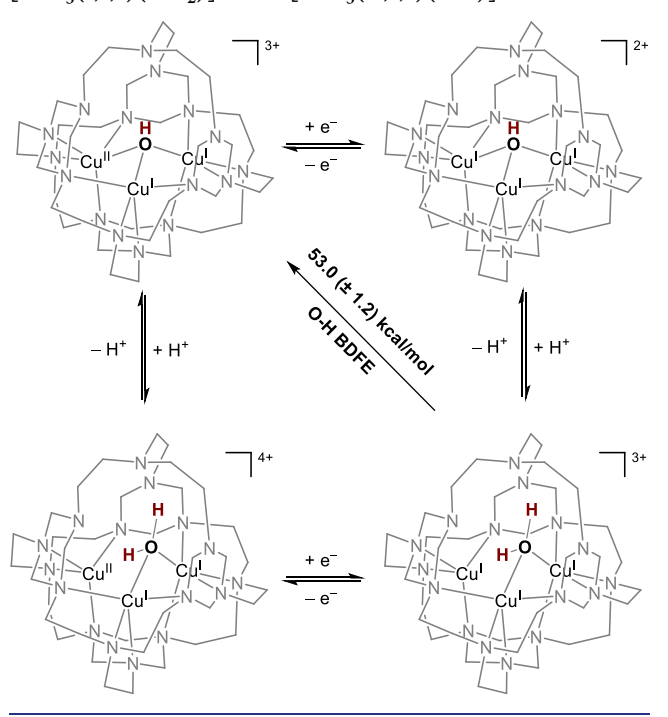
determine the BDFE of O–H and N–H motifs using the Bordwell equation. 30,31

BDFE(X - H) =
$$1.37pK_a + 23.06E^{\circ} + C_g$$
 (1)

In this equation, pK_a represents the acid dissociation constant of the acidic proton in the X–H bond, E° represents the standard reduction potential of the redox couple associated with the X–H bond, and C_g is a constant that relates to the reduction potential of H^+/H^{\bullet} in the solvent of interest.

This method of BDFE analysis is most appropriate for systems with at least three stable species in a square scheme (Scheme 1),

Scheme 1. PCET Square Scheme That Connects Complexes [LCu₃(I,I,I)(OH₂)]³⁺ and [LCu₃(II,I,I)(OH)]³⁺



allowing for experimental determination of $E_{1/2}$ and pK_a . Although many tricopper intermediates were isolated, we could not measure the pK_a of O–H and N–H groups using standard acid—base titration because the O–H and N–H motifs are buried inside the cage-like ligand construct. Treatment of the tricopper cluster with an acid or base often leads to disproportionation reactions.

Recent work by Mayer et al. demonstrated an alternative approach to determine the BDFE of the X–H bond using electrochemical OCP measurements. The BDFE of X–H bonds was determined by measuring the OCP of solutions containing varying ratios of reduced and oxidized compounds in a buffer. The purpose of the buffer is to minimize the effects of homoconjugation on the proton activity of the solution and prevent deviations from the expected behavior described by the Nernst equation 35,36

$$E = E^{\circ} - \frac{0.0592}{n} \log \frac{[XH_n][A^{-}]^n}{[X][HA]^n} - 0.059pK_a$$
 (2)

where n represents the number of proton—electron pairs transferred, $[XH_n]$ and [X] represent the concentrations of the reduced and oxidized partners, and [HA] and $[A^-]$ are the

concentrations of the buffer system; pK_a is the acid dissociation constant of the buffer used.

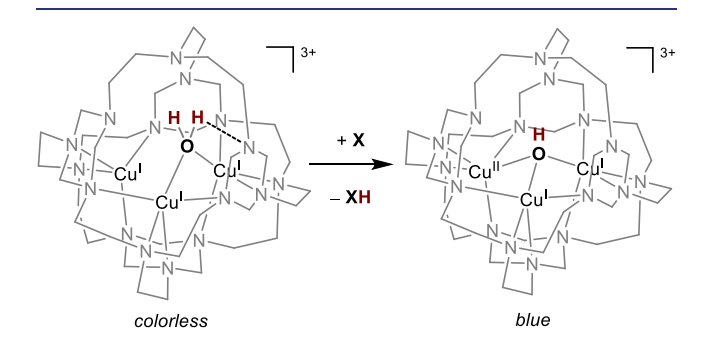
Accordingly, the OCP was collected for various ratios of $[LCu_3(I,I,I)(OH_2)]^{3+}/[LCu_3(II,I,I)(OH)]^{3+}$ in the presence of pyridinium/pyridine buffer $(pK_a=12.53)$ in acetonitrile. $[LCu_3(I,I,I)(OH_2)]^{3+}$ and $[LCu_3(II,I,I)(OH)]^{3+}$ were prepared according to literature procedures. ^{8,24} These two tricopper clusters are related by the square scheme in Scheme 1. By referencing the potentials measured against the H^+/H_2 couple, the BDFE(O-H) of the tricopper(I,I,I) aqua moiety can be calculated using eq 3

BDFE(X - H) =
$$23.06E_{OCP}^{\circ}(V \text{ vs H}^{+}/H_{2})$$

+ $\Delta G^{\circ}(\frac{1}{2}H_{2}(g)/H_{1M})$ (3)

where E°_{OCP} is the OCP measured for a 1:1 mixture of a reduced and oxidized cluster and ΔG° is a constant related to the free energy of homolytic cleavage of H_2 in acetonitrile ($\Delta G^{\circ} = 52.0 \, \text{kcal/mol}$). From this calculation, we obtained an BDFE(O–H) of 53.0 (±1.2) kcal/mol for [LCu₃(I,I,I)(OH₂)]³⁺ in acetonitrile (see Supporting Information, Figure S2).

To further corroborate the 53.0 (± 1.2) kcal/mol BDFE(O–H) value, we conducted a reactivity study of [LCu₃(I,I,I)- (OH_2)]³⁺ with various hydrogen atom-accepting reagents in acetonitrile (Figure 4). All HAT reactions were performed for an



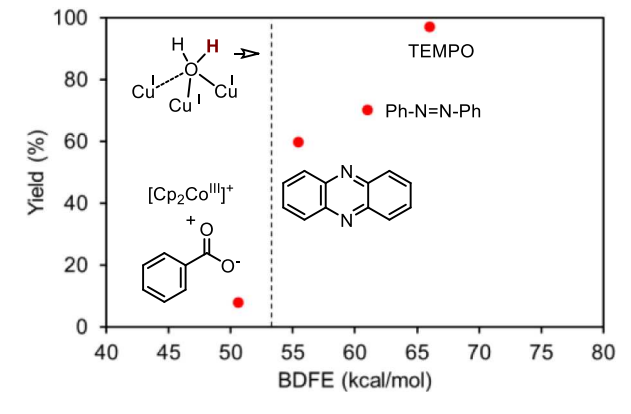


Figure 4. Yields of HAT reaction from $[LCu_3(I,I,I)(OH_2)]^{3+}$ to various hydrogen atom acceptors. The dashed line denotes 53.0 kcal/mol, the experimentally determined BDFE of the $[LCu_3(I,I,I)(OH_2)]^{3+}$ complex.

extended period of 16 h to ensure that they had reached equilibria (see Supporting Information). Treatment of $[LCu_3(I,I,I)(OH_2)]^{3+}$ with one equivalent of TEMPO [BDFE-(O-H) of TEMPOH = 66 kcal/mol] at 20 °C leads to a distinct color change from colorless to blue, corresponding to the oxidized cluster $[LCu_3(II,I,I)(OH)]^{3+}$. The absorption feature

at 790 nm (840 M⁻¹ cm⁻¹) was used to determine the yield as 97%. The formation of TEMPO-H was confirmed by ¹H NMR analysis in 91% yield. Similarly, the reaction of [LCu₃(I,I,I)-(OH₂)]³⁺ with azobenzene leads to the formation of 1,2diphenylhydrazine [BDFE(N-H) = 61 kcal/mol] and the oxidized cluster [LCu₃(II,I,I)(OH)]³⁺ in 71% yield. The formation of 1,2-diphenylhydrazine was confirmed by ¹H NMR analysis in 66% yield. Moreover, the reaction of the reduced cluster with phenazine produced the oxidized cluster in 60% yield, indicating that the BDFE of $[LCu_3(I,I,I)(OH_2)]^{3+}$ is close to 58 kcal/mol. The formation of a 5,10-dihydrophenazine product [BDFE(O-H) = 58.7 kcal/mol] was confirmed by ${}^{1}H$ NMR analysis in 63% yield. Finally, we investigated the reactivity of [LCu₃(I,I,I)(OH₂)]³⁺ toward the reduction of cobaltocenium hexafluorophosphate ($Cp_2Co^{III}PF_6$, $E_{1/2}$ = -1.34) in the presence of sodium benzoate (p $K_a = 21.51$) as a base. The combination of these two reagents affords an effective BDFE of 50.6 kcal/mol. ^{37,38} As the BDFE(O-H) value of $[LCu_3(I,I,I)(OH_2)]^{3+}$ is higher than 50.6 kcal/mol, we did not observe a significant reduction of Cp₂Co^{III}PF₆ (8%) after 16 h. These reactivity studies of [LCu₃(I,I,I)(OH₂)]³⁺ provide additional support to a BDFE(O-H) value of 53.0 kcal/mol.

Redox Potentials of Tricopper μ -OH₂ and μ -OH Complexes. The redox potentials $(E_{1/2})$ of the tricopper cluster were determined by solution cyclic voltammetry (CV) studies. Previously, we reported the CV of tricopper clusters at one-proton and two-proton levels. ^{8,24} The intramolecular proton transfer between the tricopper cluster and the secondary coordination sphere N/N-H motif makes certain redox events irreversible. Nevertheless, at high scan rates or at low temperatures, the reversibility improves. This method allowed us to measure seven $E_{1/2}$ values in the PCET square schemes (Table 1; see Supporting Information for details).

Table 1. Summary of Redox Potentials of Tricopper Clusters

	$E_{1/2}^{a}(V)$	method	refs
[LHCu ₃ O] ^{5+/4+}	-0.66	CV at high scan rate	ref 24
$[LHCu_3O]^{4+/3+}$	-1.18^{b}	CV at −40°C	this work
$[LCu_3OH]^{5+/4+}$	-0.13	CV at −40°C	ref 24
$[LCu_3OH]^{4+/3+}$	-0.52	CV at RT	ref 24
$[LCu_3OH]^{3+/2+}$	-0.98	CV at RT	ref 24
$[LCu_3OH_2]^{4+/3+}$	-0.30^{b}	CV at −40°C	this work
$[LCu_3OH_2]^{5+/4+}$	0.01 ^b	CV at −40°C	this work
$[LHCu_3OH]^{4+/3+}$	-0.66	CV at RT	ref 24
$[LHCu_3OH]^{5+}/^{4+}$	-0.27	CV at RT	ref 24
[LHCu ₃ OH] ^{6+/5+}	0.17	CV at RT	ref 24

 $^a\mathrm{Referenced}$ to Fc⁺/Fc. $^b\mathrm{Irreversible}$ redox couples. The $E_{1/2}$ values are estimated using the method of inflection potentials. 39,40

In this study, we performed additional low-temperature CV studies to estimate the $E_{1/2}$ of three redox couples, namely, $[LHCu_3O]^{4+/3+}$, $[LCu_3OH_2]^{5+/4+}$, and $[LCu_3OH_2]^{4+/3+}$. We prepared the CV sample using the copper clusters that have the correct "protonation state", cooled the CV sample down to -40 °C to slow down the intramolecular transfer, and then measured their redox potential using CV. For redox couples that do not exhibit reversible CV features, we estimated the $E_{1/2}$ values using the inflection potentials. ^{39,40} The resulting redox potentials are summarized in Table 1.

These redox potential values, along with the BDFE(O-H) value of $[LCu_3(I,I,I)(OH_2)]^{3+}$, allowed us to calculate the BDFE(O-H) at other oxidation states using the Bordwell

equation and the redox potentials of clusters (Figure 5A). Additionally, we were able to determine the pK_a values of three tricopper aqua complexes as -3.57 for [LCu₃(II,II,I)(OH₂)]^{S+}, 5.34 for [LCu₃(II,I,I)(OH₂)]⁴⁺, and 16.8 for [LCu₃(I,I,I)-(OH₂)]³⁺, respectively. The basicity of the O–H group increases by 8–11 pK_a units per oxidation state (Figure 5A), providing significant driving forces for intramolecular proton transfer from the secondary coordination sphere as the tricopper center is reduced.

O-H BDFE of Tricopper μ -OH Complexes. Similarly, the BDFE(O-H) of [LHCu₃(II,II,I)(OH)]⁵⁺ was determined by OCP measurement of various ratios of [LHCu₃(II,II,I)(OH)]⁵⁺ and [LHCu₃(II,II,II)(O)]⁵⁺ (Scheme 2) in the presence of 2,4dinitrobenzenesulfonic acid/2,4-dinitrobenzenesulfonic acid potassium salt buffer ($pK_a = 3.96$) in acetonitrile. These two tricopper clusters were prepared according to previously reported procedures. ^{8,24} Using eq 3, we obtained a BDFE(O–H) for [LHCu₃(II,II,I)(OH)]⁵⁺ of 57.1 (±1.11) kcal/mol in acetonitrile (see Supporting Information, Figure S4). Analogously, this BDFE(O-H) value enabled us to calculate the BDFE(O-H) and $pK_a(O-H)$ of the adjacent square schemes using the Bordwell equation (Figure 5B). With each oxidation state change, the basicity of the OH group in tricopper μ -oxo/ hydroxo complexes increases by 14-16 pK₂ units. This substantial increase in basicity provides the driving force for intramolecular proton transfer from the secondary coordination sphere.

BDFE of N–H Bonds in the Secondary Coordination Sphere. After establishing the BDFE(O–H) of tricopper oxo/hydroxo/aqua species at different oxidation states, we sought to investigate the BDFE(N–H) of the secondary coordination sphere (Figure 5C). Previously, using CV simulation of [LCu₃(I,I,I)(OH₂)]³⁺, we estimated the K_{eq} of intramolecular proton transfer between [LHCu₃(II,I,I)(OH)]⁴⁺ and [LCu₃(II,I,I)(OH₂)]⁴⁺ as 6.5×10^{-6} (Figure 6A).²⁴ Given a p K_a (O–H) value of [LCu₃(II,I,I)(OH₂)]⁴⁺ of 5.34 (±1.21) (Figure 5A), we can estimate the p K_a (N–H) of [LHCu₃(II,I,I)(OH)]⁴⁺ in the range between 8.45 and 11.37 (Figure 6A).

To further validate this $pK_a(N-H)$ estimation, we treated $[LCu_3(II,I,I)(OH)]^{3+}$ with acids of various strengths and monitored its conversion to [LHCu₃(II,I,I)(OH)]⁴⁺ (Figure 6B). The formation of $[LHCu_3(II,I,I)(OH)]^{4+}$ can be confirmed using its redox feature at -0.27 V vs Fc⁺/Fc.^{8,24} We found that the treatment of [LCu₃(II,I,I)(OH)]³⁺ with one equivalent of trichloroacetic acid (p $K_a = 10.75$) in acetonitrile leads to the formation of [LHCu₃(II,I,I)(OH)]⁴⁺, as indicated by the cyclic voltammogram (see Supporting Information, Figure S19). 8,24 In contrast, treatment of [LCu₃(II,I,I)(OH)]³⁺ with pyridinium tetrafluoroborate (p $K_a = 12.53$) in acetonitrile with $[LCu_3(II,I,I)(OH)]^{3+}$ does not result in any changes in the voltammogram, indicating that the $pK_a(N-H)$ of [LHCu₃(II,I,I)(OH)]³⁺ is lower than 12.53 (see Supporting Information, Figure S19). These studies are consistent with the pK_a(N-H) between 8.45 and 11.37 estimated by CV simulation.

Using a $pK_a(N-H)$ value for $[LHCu_3(II,I,I)(OH)]^{3+}$, the BDFE(N-H) and $pK_a(N-H)$ of the secondary sphere N-H bond at different oxidation states can be calculated using the Bordwell equation. The results are summarized in Figure 5C.

DISCUSSIONS AND CONCLUSIONS

The ability of MCOs to catalyze ORR while avoiding oxidative damage highlights the importance of understanding the

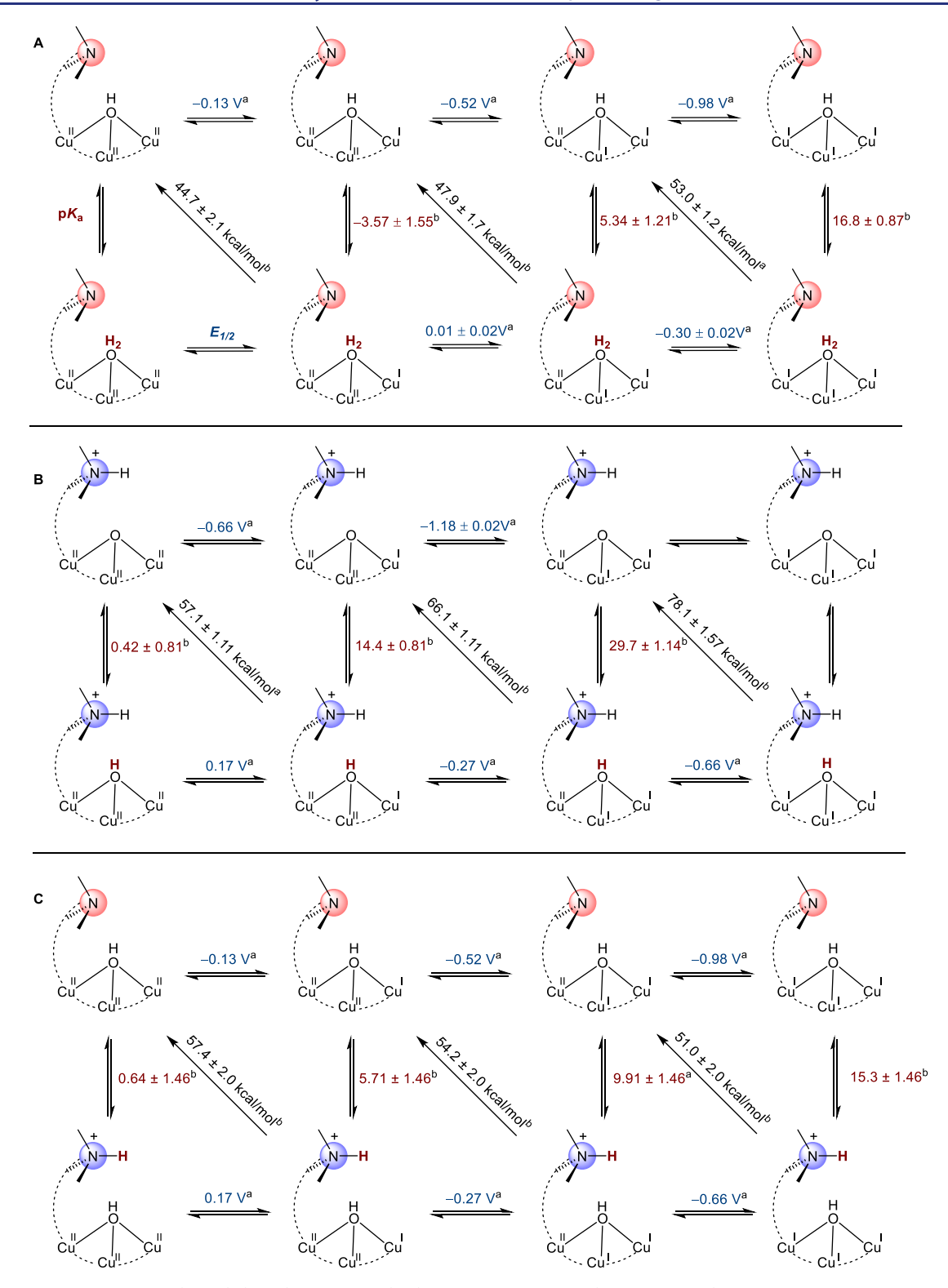
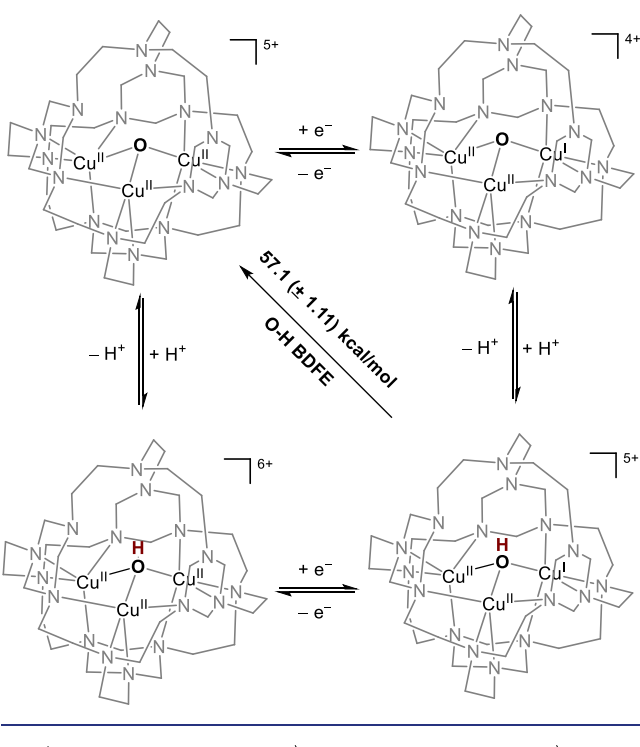


Figure 5. Summary of the BDFE(O–H) (black), pK_a values (red), and redox potentials (blue, vs Fc⁺/Fc) at different oxidation states. The TREN₄ ligand is omitted for clarity. The tertiary nitrogen above the cluster indicates the proton storage site in the secondary coordination sphere. (A) PCET at the tricopper complex from LCu₃(II,II,II)OH to LCu₃(I,I,I)OH₂, with tertiary nitrogen being deprotonated. (B) PCET at the tricopper complex from LHCu₃(II,II,II)OH to LHCu₃(I,I,I)OH with tertiary nitrogen being protonated. (C) Multisite PCET at the tricopper complex from LCu₃(II,II,II)OH to LHCu₃(I,I,I)OH, with electron transfer at the tricopper center and proton transfer at tertiary nitrogen at the secondary coordination sphere. ^aValues obtained from direct experimental measurements. ^bValues calculated using the Bordwell equation. The relative uncertainties derived from OCP measurement and estimation of $E_{1/2}$ have been extended to all the calculated values of BDFE and pK_a .

mechanisms of MCOs at the molecular level. Despite the simplicity of the tricopper model complexes, they provide insights into PCET conversion of Cu₃(II,II,II)O to Cu₃(I,I,I)-

 OH_2 species. This process mimics the reductive regeneration of RO to FR in MCOs. The top TREN motif, which is ca. 3.98 Å away from the tricopper cluster, serves as a pendant proton relay,

Scheme 2. PCET Square Scheme That Connects Complexes [LHCu₃(II,II,I)(OH)]⁵⁺ and [LHCu₃(II,II,II)(O)]⁵⁺



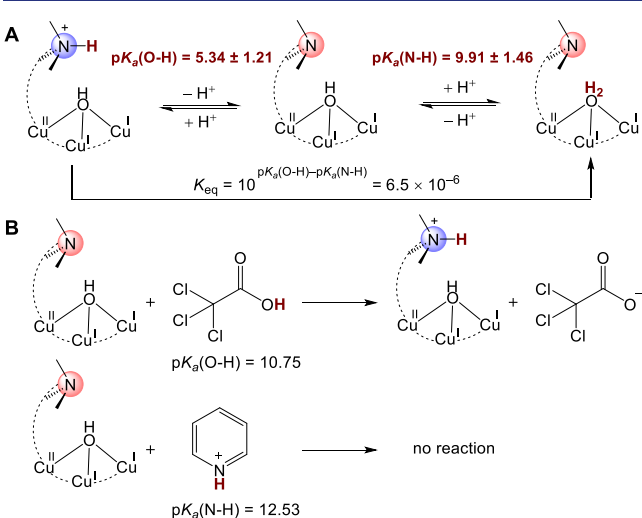


Figure 6. (A) PT equilibria between $[LHCu_3(II,I,I)(OH)]^{4+}$, $[LCu_3(II,I,I)(OH)]^{3+}$, and $[LCu_3(II,I,I)(OH_2)]^{4+}$. (B) Protonation of $[LCu_3(II,I,I)(OH)]^{3+}$ with trichloroacetic acid and pyridinium tetrafluoroborate.

mimicking the functions of carboxylate groups adjacent to the biological tricopper center (ca. 4.00 Å, Figure 1A).

The p K_a values of O–H and N–H motifs determine the protonation states of the tricopper center and the proton relay at the secondary coordination sphere. Although the N–H group is not covalently bonded to the tricopper center, its p K_a value still increases significantly by ca. 5 p K_a units per oxidation state (Figure 7, red trace). This observation reflects the electrostatic influences of metallocofactors on the p K_a of the surrounding amino acid residues.⁴¹

Due to the proximity of OH and OH_2 ligands, their pK_a values are significantly influenced by the charge/oxidation state of the tricopper center. This is evident in the 14-16 pK_a increase for

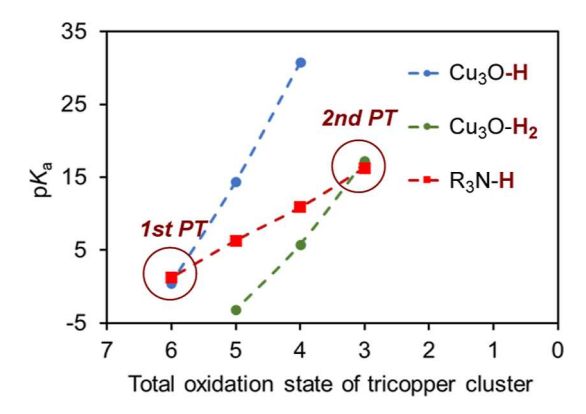


Figure 7. Plots of pK_a of O–H and N–H motifs against the oxidation state of the tricopper center.

OH (Figure 7, blue trace) and 8-11 pK_a increase for OH₂ per oxidation state change (Figure 7, green trace). A similar study by Agapie and Reed on the Fe₃Mn aqua cluster and Fe₄ hydroxo cluster shows a change of 4-8 pK_a(O-H) units per oxidation state. ^{42,43}

The consequence of these pK_a trends in Figure 7 is that, as the tricopper center is reduced, the basicity of the tricopper oxo/hydroxo sites (blue and green traces) increases faster than the secondary coordination sphere N–H motif (red trace), resulting in two intersection points. These two intersection points (red circles, Figure 7) indicate where the basicity of the Cu_3 cluster surpasses that of the N–H motif in the secondary coordination sphere, providing driving forces for proton transfer to the tricopper center.

Worth noting is the trend of BDFE(O-H) along the $3e^-2H^+$ PCET conversion of LHCu₃(II,II,II)O to LCu₃(I,I,I)OH₂ species. The tricopper species on the ideal path of alternating electron and proton transfer (ET-PT-ET-PT-ET) exhibit mild BDFE(O-H) values around 53.0-57.1 kcal/mol (Figure 8). In

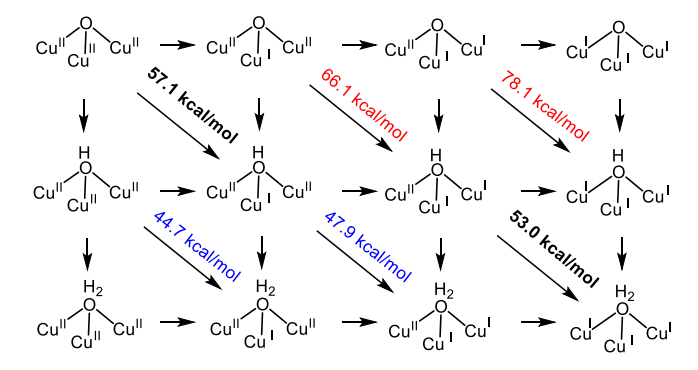


Figure 8. Summary of BDFE(O-H) values at the tricopper cluster.

contrast, those not on the ET-PT-ET-PT-ET path have either much lower (44.7 kcal/mol) or higher (78.1 kcal/mol) BDFE(O-H) values (Figure 8). In the context of biological O₂ reduction at the tricopper center, our study highlights the "safest" PCET pathways with the least reactive tricopper intermediates. The tricopper species along the diagonal pathway tend to be less reactive toward C-H activation (high O-H BDFEs) or production of ROS (low O-H BDFEs), both of which can lead to cellular damage. These results suggest that the BDFE(O-H) should be considered when designing bioinspired ORR catalysts with high efficiency and specificity.

In contrast to the significant changes of BDFE (O–H) values, the BDFE values of the N–H bond in the secondary coordination sphere exhibit minimal variations, ranging from 51 to 58 kcal/mol, despite notable shifts in p $K_{\rm a}$ (>14 p $K_{\rm a}$ units) and $E_{1/2}$ changes (>1000 mV). This trend aligns with the findings from Yang et al.'s investigation into the N–H BDFE of manganese imido complexes appended with a crown ether unit containing Lewis acid metal cations. ^{44,45} These two studies collectively highlight the efficacy of modifying adjacent charge moieties as a strategy to alter the p $K_{\rm a}$ values of X–H while preserving BDFE values.

In the tricopper aqua (Cu_3OH_2) system, we observed a decrease in BDFE(O–H) by 4–6 kcal/mol per increment in the oxidation state. In the tricopper hydroxo (Cu_3OH) system, this decrease of BDFE(O–H) is more pronounced, ranging from 9 to 12 kcal/mol per oxidation state increase. These findings are in contrast to those reported by Agapie and Reed, who observed an increase in BDFE(O–H) with higher oxidation states in Fe₄OH clusters and Fe₃MnOH₂ clusters (increments of 4–7 kcal/mol per oxidation state). 42,43

To elucidate this difference, we partition the BDFE changes into two key contributing factors: redox potential ($nF\Delta E_{1/2}$, Figure 9, blue bars) and basicity/acidity ($RT\ln\Delta pK_a$, Figure 9, red bars). The cumulative effect of these two opposing influences determines the overall BDFE trend (Figure 9, gray

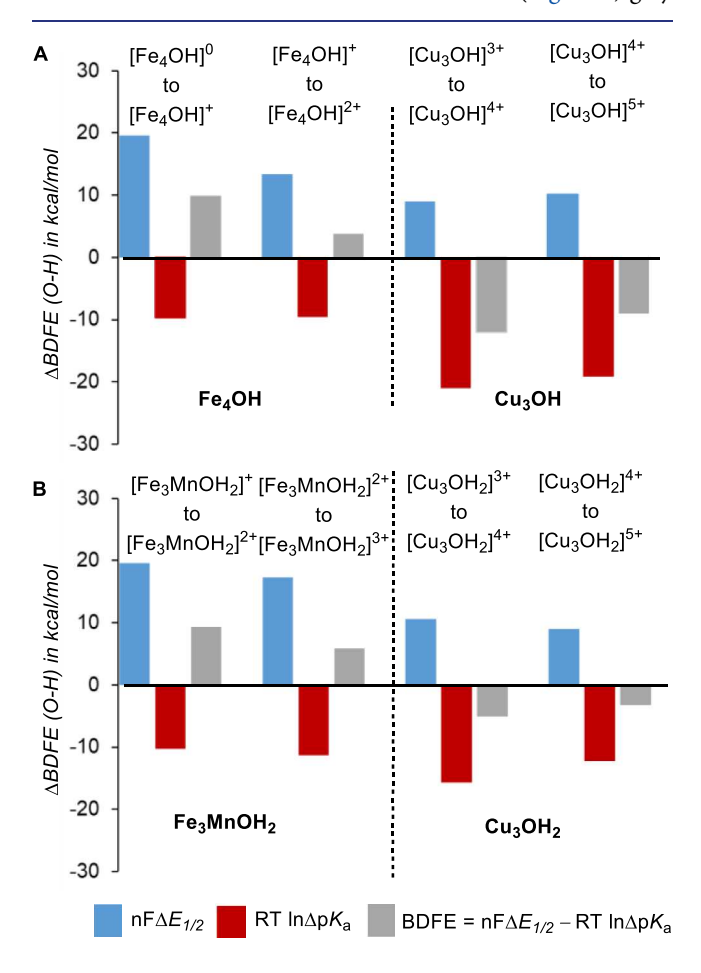


Figure 9. Summary of the contribution of $\Delta E_{1/2}$ (blue) and $\Delta p K_a$ (red) toward the overall change in BDFE (gray) at different oxidation states. (A) Comparison of BDFE(O-H) of Fe₄OH vs Cu₃OH at different oxidation states. (B) Comparison of BDFE(O-H) of Fe₃MnOH₂ vs Cu₃OH₂ at different oxidation states.

bars), which trends positive for Fe₃Mn and Fe₄ clusters but trends negative for tricopper clusters. Figure 9 underscores the greater impact of redox potential on the BDFE(O–H) of Fe₃Mn and Fe₄ clusters and the stronger influence of p K_a on the BDFE(O–H) of tricopper clusters. A similar dominance of p K_a contribution to BDFE(O–H) has been noted in the dicopper hydroxo/oxo system studied by Kieber-Emmons.²⁷ These varying trends of BDFE as a function of the cluster oxidation state may arise from (1) inherent differences in mid vs late transition metals, (2) binding mode of oxo/hydroxo/aqua ligands, or (3) the overall charge of the cluster. These factors will be the topic of future investigation.

ASSOCIATED CONTENT

Supporting Information

The Supporting Information is available free of charge at https://pubs.acs.org/doi/10.1021/jacs.3c14420.

Experimental details, including characterization data, spectra, and results (PDF)

AUTHOR INFORMATION

Corresponding Author

Shiyu Zhang — Department of Chemistry & Biochemistry, The Ohio State University, Columbus, Ohio 43210, United States; orcid.org/0000-0002-2536-4324; Email: zhang.8941@osu.edu

Authors

Saikat Mondal – Department of Chemistry & Biochemistry, The Ohio State University, Columbus, Ohio 43210, United States Weiyao Zhang – Department of Chemistry & Biochemistry, The Ohio State University, Columbus, Ohio 43210, United States

Complete contact information is available at: https://pubs.acs.org/10.1021/jacs.3c14420

Notes

The authors declare no competing financial interest.

ACKNOWLEDGMENTS

This publication is based on work funded by the National Science Foundation under award no. CHE-1904560.

REFERENCES

- (1) Solomon, E. I.; Sundaram, U. M.; Machonkin, T. E. Multicopper Oxidases and Oxygenases. *Chem. Rev.* **1996**, *96*, 2563–2606.
- (2) Mayer, A. M.; Staples, R. C. Laccase: New Functions for an Old Enzyme. *Phytochemistry* **2002**, *60*, 551–565.
- (3) Hullo, M. F.; Moszer, I.; Danchin, A.; Martin-Verstraete, I. CotA of Bacillus Subtilis Is a Copper-Dependent Laccase. *J. Bacteriol.* **2001**, 183, 5426–5430.
- (4) Sekretareva, A.; Tian, S.; Gounel, S.; Mano, N.; Solomon, E. I. Electron Transfer to the Trinuclear Copper Cluster in Electrocatalysis by the Multicopper Oxidases. *J. Am. Chem. Soc.* **2021**, *143*, 17236–17249.
- (5) Heppner, D. E.; Kjaergaard, C. H.; Solomon, E. I. Mechanism of the Reduction of the Native Intermediate in the Multicopper Oxidases: Insights into Rapid Intramolecular Electron Transfer in Turnover. *J. Am. Chem. Soc.* **2014**, *136*, 17788–17801.
- (6) Sekretaryova, A.; Jones, S. M.; Solomon, E. I. O² Reduction to Water by High Potential Multicopper Oxidases: Contributions of the T1 Copper Site Potential and the Local Environment of the Trinuclear Copper Cluster. *J. Am. Chem. Soc.* **2019**, *141*, 11304–11314.

- (7) Cole, A. P.; Root, D. E.; Mukherjee, P.; Solomon, E. I.; Stack, T. D. P. A Trinuclear Intermediate in the Copper-Mediated Reduction of O₂: Four Electrons from Three Coppers. *Science* **1996**, 273, 1848–1850.
- (8) Zhang, W.; Moore, C. E.; Zhang, S. Encapsulation of Tricopper Cluster in a Synthetic Cryptand Enables Facile Redox Processes from Cu^ICu^ICu^I to Cu^{II}Cu^{II} States. *Chem. Sci.* **2021**, *12*, 2986–2992.
- (9) Singha, A.; Sekretareva, A.; Tao, L.; Lim, H.; Ha, Y.; Braun, A.; Jones, S. M.; Hedman, B.; Hodgson, K. O.; Britt, R. D.; Kosman, D. J.; Solomon, E. I. Tuning the Type 1 Reduction Potential of Multicopper Oxidases: Uncoupling the Effects of Electrostatics and H-Bonding to Histidine Ligands. *J. Am. Chem. Soc.* 2023, 145, 13284–13301.
- (10) Solomon, E. I.; Heppner, D. E.; Johnston, E. M.; Ginsbach, J. W.; Cirera, J.; Qayyum, M.; Kieber-Emmons, M. T.; Kjaergaard, C. H.; Hadt, R. G.; Tian, L. Copper Active Sites in Biology. *Chem. Rev.* **2014**, *114*, 3659–3853.
- (11) Palmer, A. E.; Lee, S. K.; Solomon, E. I. Decay of the Peroxide Intermediate in Laccase: Reductive Cleavage of the O- O Bond. *J. Am. Chem. Soc.* **2001**, *123*, 6591–6599.
- (12) Yoon, J.; Solomon, E. I. Electronic Structure of the Peroxy Intermediate and Its Correlation to the Native Intermediate in the Multicopper Oxidases: Insights into the Reductive Cleavage of the O-O Bond. J. Am. Chem. Soc. 2007, 129, 13127–13136.
- (13) Kjaergaard, C. H.; Durand, F.; Tasca, F.; Qayyum, M. F.; Kauffmann, B.; Gounel, S.; Suraniti, E.; Hodgson, K. O.; Hedman, B.; Mano, N.; Solomon, E. I. Spectroscopic and Crystallographic Characterization of "Alternative Resting" and "Resting Oxidized" Enzyme Forms of Bilirubin Oxidase: Implications for Activity and Electrochemical Behavior of Multicopper Oxidases. *J. Am. Chem. Soc.* **2012**, *134*, 5548–5551.
- (14) Palmer, A. E.; Quintanar, L.; Severance, S.; Wang, T. P.; Kosman, D. J.; Solomon, E. I. Spectroscopic Characterization and O₂ Reactivity of the Trinuclear Cu Cluster of Mutants of the Multicopper Oxidase Fet3p. *Biochemistry* **2002**, *41*, 6438–6448.
- (15) Engelmann, X.; Farquhar, E. R.; England, J.; Ray, K. Four-Electron Reduction of Dioxygen to Water by a Trinuclear Copper Complex. *Inorg. Chim. Acta* **2018**, *481*, 159–165.
- (16) Jones, S. M.; Heppner, D. E.; Vu, K.; Kosman, D. J.; Solomon, E. I. Rapid Decay of the Native Intermediate in the Metallooxidase Fet3p Enables Controlled Fe^{II} Oxidation for Efficient Metabolism. *J. Am. Chem. Soc.* **2020**, *142*, 10087–10101.
- (17) Suh, M. P.; Han, M. Y.; Lee, J. H.; National, S.; Uni, V. One-Pot Template Synthesis and Properties of a Molecular Bowl: Dodecaaza Macrotetracycle with μ_3 -Oxo and μ_3 -Hydroxo Tricopper (II) Cores. *J. Am. Chem. Soc.* **1998**, *120*, 3819–3820.
- (18) Gupta, A. K.; Tolman, W. B. Cu(I)/O₂ Chemistry Using a β -Diketiminate Supporting Ligand Derived from *N*,*N*-Dimethylhydrazine: A $[Cu_3O_2]^{3+}$ Complex with Novel Reactivity. *Inorg. Chem.* **2012**, *51*, 1881–1888.
- (19) Lionetti, D.; Day, M. W.; Agapie, T. Metal-Templated Ligand Architectures for Trinuclear Chemistry: Tricopper Complexes and Their O₂ Reactivity. *Chem. Sci.* **2013**, *4*, 785–790.
- (20) Cook, B. J.; Di Francesco, G. N.; Kieber-Emmons, M. T.; Murray, L. J. A Tricopper(I) Complex Competent for O Atom Transfer, C-H Bond Activation, and Multiple O2 Activation Steps. *Inorg. Chem.* **2018**, *57*, 11361–11368.
- (21) Taki, M.; Teramae, S.; Nagatomo, S.; Tachi, Y.; Kitagawa, T.; Itoh, S.; Fukuzumi, S. Fine-Tuning of Copper(I)-Dioxygen Reactivity by 2-(2-Pyridyl)Ethylamine Bidentate Ligands. *J. Am. Chem. Soc.* **2002**, 124, 6367–6377.
- (22) Tsui, E. Y.; Day, M. W.; Agapie, T. Trinucleating Copper: Synthesis and Magnetostructural Characterization of Complexes Supported by a Hexapyridyl 1,3,5-Triarylbenzene Ligand. *Angew. Chem., Int. Ed.* **2011**, *50*, 1668–1672.
- (23) Brown, E. C.; Johnson, B.; Palavicini, S.; Kucera, B. E.; Casella, L.; Tolman, W. B. Modular Syntheses of Multidentate Ligands with Variable N-Donors: Applications to Tri- and Tetracopper(i) Complexes. J. Chem. Soc., Dalton Trans. 2007, No. 28, 3035–3042.
- (24) Zhang, W.; Moore, C. E.; Zhang, S. Multiple Proton-Coupled Electron Transfers at a Tricopper Cluster: Modeling the Reductive

- Regeneration Process in Multicopper Oxidases. J. Am. Chem. Soc. 2022, 144, 1709–1717.
- (25) Dhar, D.; Tolman, W. B. Hydrogen Atom Abstraction from Hydrocarbons by a Copper(III)-Hydroxide Complex. *J. Am. Chem. Soc.* **2015**, *137*, 1322–1329.
- (26) Ali, G.; Vannatta, P. E.; Ramirez, D. A.; Light, K. M.; Kieber-Emmons, M. T. Thermodynamics of a μ -Oxo Dicopper(II) Complex for Hydrogen Atom Abstraction. *J. Am. Chem. Soc.* **2017**, *139*, 18448–18451.
- (27) VanNatta, P. E.; Ramirez, D. A.; Velarde, A. R.; Ali, G.; Kieber-Emmons, M. T. Exceptionally High O-H Bond Dissociation Free Energy of a Dicopper(II) μ -Hydroxo Complex and Insights into the Geometric and Electronic Structure Origins Thereof. *J. Am. Chem. Soc.* **2020**, *142*, 16292–16312.
- (28) Quist, D. A.; Ehudin, M. A.; Schaefer, A. W.; Schneider, G. L.; Solomon, E. I.; Karlin, K. D. Ligand Identity-Induced Generation of Enhanced Oxidative Hydrogen Atom Transfer Reactivity for a $Cu^{II}_{2}(O_{2}^{\bullet -})$ Complex Driven by Formation of a CuII2(-OOH) Compound with a Strong O-H Bond. *J. Am. Chem. Soc.* 2019, 141, 12682–12696.
- (29) Kindermann, N.; Günes, C. J.; Dechert, S.; Meyer, F. Hydrogen Atom Abstraction Thermodynamics of a μ -1,2-Superoxo Dicopper(II) Complex. *J. Am. Chem. Soc.* **2017**, *139*, 9831–9834.
- (30) Bordwell, F. G.; Cheng, J.-P.; Harrelson, J. A. Homolytic bond dissociation energies in solution from equilibrium acidity and electrochemical data. *J. Am. Chem. Soc.* **1988**, *110*, 1229–1231.
- (31) Bordwell, F. G.; Liu, W. Z. Solvent Effects on Homolytic Bond Dissociation Energies of Hydroxylic Acids. *J. Am. Chem. Soc.* **1996**, *118*, 10819–10823.
- (32) Wise, C. F.; Agarwal, R. G.; Mayer, J. M. Determining Proton-Coupled Standard Potentials and X-H Bond Dissociation Free Energies in Nonaqueous Solvents Using Open-Circuit Potential Measurements. *J. Am. Chem. Soc.* **2020**, *142*, 10681–10691.
- (33) Fertig, A. A.; Brennessel, W. W.; McKone, J. R.; Matson, E. M. Concerted Multiproton-Multielectron Transfer for the Reduction of O_2 to H_2O with a Polyoxovanadate Cluster. *J. Am. Chem. Soc.* **2021**, *143*, 15756–15768.
- (34) Wu, T.; Rajabimoghadam, K.; Puri, A.; Hebert, D. D.; Qiu, Y. L.; Eichelberger, S.; Siegler, M. A.; Swart, M.; Hendrich, M. P.; Garcia-Bosch, I. A 4H⁺/4e⁻ Electron-Coupled-Proton Buffer Based on a Mononuclear Cu Complex. *J. Am. Chem. Soc.* **2022**, *144*, 16905–16915.
- (35) Roberts, J. A. S.; Bullock, R. M. Direct Determination of Equilibrium Potentials for Hydrogen Oxidation/Production by Open Circuit Potential Measurements in Acetonitrile. *Inorg. Chem.* **2013**, *52*, 3823–3835.
- (36) Appel, A. M.; Helm, M. L. Determining the Overpotential for a Molecular Electrocatalyst. *ACS Catal.* **2014**, *4*, 630–633.
- (37) Warren, J. J.; Tronic, T. A.; Mayer, J. M. Thermochemistry of Proton-Coupled Electron Transfer Reagents and Its Implications. *Chem. Rev.* **2010**, *110*, 6961–7001.
- (38) McCarthy, B. D.; Martin, D. J.; Rountree, E. S.; Ullman, A. C.; Dempsey, J. L. Electrochemical Reduction of Brønsted Acids by Glassy Carbon in Acetonitrile—Implications for Electrocatalytic Hydrogen Evolution. *Inorg. Chem.* **2014**, *53*, 8350–8361.
- (39) Espinoza, E. M.; Clark, J. A.; Soliman, J.; Derr, J. B.; Morales, M.; Vullev, V. I. Practical Aspects of Cyclic Voltammetry: How to Estimate Reduction Potentials When Irreversibility Prevails. *J. Electrochem. Soc.* **2019**, *166*, H3175—H3187.
- (40) Bower, J. K.; Reese, M. S.; Mazin, I. M.; Zarnitsa, L. M.; Cypcar, A. D.; Moore, C. E.; Sokolov, A. Y.; Zhang, S. C(sp³)-H Cyanation by a Formal Copper(III) Cyanide Complex. *Chem. Sci.* **2023**, *14*, 1301–1307.
- (41) Louro, R. O.; Catarino, T.; Paquete, C. M.; Turner, D. L. Distance Dependence of Interactions between Charged Centres in Proteins with Common Structural Features. *FEBS Lett.* **2004**, *576*, 77–80.
- (42) Reed, C. J.; Agapie, T. A Terminal Fe^{III}-Oxo in a Tetranuclear Cluster: Effects of Distal Metal Centers on Structure and Reactivity. *J. Am. Chem. Soc.* **2019**, *141*, 9479–9484.

- (43) Reed, C. J.; Agapie, T. Thermodynamics of Proton and Electron Transfer in Tetranuclear Clusters with Mn-OH₂/OH Motifs Relevant to H₂O Activation by the Oxygen Evolving Complex in Photosystem II. *J. Am. Chem. Soc.* **2018**, *140*, 10900–10908.
- (44) Léonard, N. G.; Chantarojsiri, T.; Ziller, J. W.; Yang, J. Y. Cationic Effects on the Net Hydrogen Atom Bond Dissociation Free Energy of High-Valent Manganese Imido Complexes. *J. Am. Chem. Soc.* **2022**, *144*, 1503–1508.
- (45) Najafian, A.; Cundari, T. R. Effect of Appended S-Block Metal Ion Crown Ethers on Redox Properties and Catalytic Activity of Mn-Nitride Schiff Base Complexes: Methane Activation. *Inorg. Chem.* **2019**, 58, 12254–12263.